Journal of Power Sources 195 (2010) 3913–3917

Contents lists available at ScienceDirect

Journal of Power Sources

journal homepage: www.elsevier.com/locate/jpowsour

Short communication

Enhanced electrochemical properties of $LiFePO_4$ cathode for Li-ion batteries with amorphous NiP coating

Gui-Ming Song[a,*], Ying Wu[b,**], Qiang Xu[c], Gang Liu[d]

[a] Department of Materials Science and Engineering, Delft University of Technology, Mekelweg 2, 2628CD Delft, The Netherlands
[b] School of Materials Science and Engineering, Shanghai Institute of Technology, Caobao Road 120, Shanghai 200081, PR China
[c] National Center for High Resolution Electron Microscopy, Delft University of Technology, Lorentzweg 1, 2628 CJ Delft, The Netherlands
[d] Department of Materials Engineering, Harbin Institute of Technology, Harbin 150001, PR China

ARTICLE INFO

Article history:
Received 21 April 2009
Received in revised form
27 November 2009
Accepted 20 December 2009
Available online 11 January 2010

Keywords:
NiP coating
$LiFePO_4$
Electrochemical property
Rate performance
Cycleability
Li-ion battery

ABSTRACT

Here we show that the intrinsic low electrical conductivity of $LiFePO_4$ which seriously hinders the application of $LiFePO_4$ for Li-ion batteries is overcome with conductive metallic NiP nano-coating. High resolution transmission electron microscopy image reveals that the NiP coating is a nanoscale amorphous layer, which was deposited on the $LiFePO_4$ particles to form a so-called core/shell structure via electroless plating at room temperature. The electrochemical performances of NiP coated $LiFePO_4$ show that both of the rate performance and cycleability of $LiFePO_4$ against graphite anode are improved by the NiP coating. Analysis of electrochemical impedance spectra of the $LiFePO_4$/graphite cells demonstrates that the NiP coating decreases both of the surface film resistance and charge transfer resistance. The dissolution of Fe from $LiFePO_4$ in the $LiPF_6$ based electrolyte is remarkably suppressed by the protective NiP coating.

1. Introduction

Compared with conventional cathode materials of Li-ion batteries, such as $LiCoO_2$, $LiNiO_2$ and $LiMn_2O_4$, olivine-type $LiFePO_4$ is very attractive due to its high theoretical capacity (170 mAh g^{-1}), a high environmental acceptability, long cycleability and low cost, and it is therefore the most promising cathode material for large-scale rechargeable batteries used for hybrid electric vehicles (HEV), in which a severe temperature environment may be experienced [1–7]. A major disadvantage of $LiFePO_4$ is its poor rate performance mainly caused by its intrinsic low electronic conductivity ($\sim 10^{-9}$ S cm^{-1} [8]), which controls the transfer of Li^+ ions upon lithium insertion/desertion [9,10]. A very effective method for improving the conductivity is to cover $LiFePO_4$ particles with conductive carbon [11–15] or add conductive metallic phases (such as Ag [16], Cu [17], and NiP particles [18], and Fe or Ni phosphide impurities [19,20]). These conductive phases work as a nanoscale conductive network surrounding $LiFePO_4$ particles, consequently enhances the electronic conductivity of $LiFePO_4$. The recent work of Li, et al. shows that the electronic conductivity of $LiFePO_4$ can be remarkably improved by three or four orders of magnitude with the addition of 0.35–1.50 wt% amorphous NiP [18]. This type of NiP contained $LiFePO_4$ was prepared via a simple one-step spraying technique, in which all the reactants were mixed in a solution and then sprayed out under compressive N_2 gas, followed by a heat treatment at about 350 °C for the synthesis of $LiFePO_4$. Probably, the formation of NiP precedes the formation of $LiFePO_4$ with this method. Thus, NiP might distribute in the $LiFePO_4$ matrix, rather than cover the surface of $LiFePO_4$ particles.

$LiFePO_4$ undergoes iron dissolution in conventional $LiPF_6$ electrolyte at relatively high temperatures (e.g. 55 and 60 °C) [21–24]. Thus, irreversible structure changes occur at the surface of $LiFePO_4$, which does not favour the Li insertion-deinsertion process. Additionally, the dissolved iron also will be reduced on the graphite anode, which catalyses the formation of a solid electrolyte interphase (SEI) layer [21]. The formation of the SEI consumes Li ions and imposes high surface resistance, both lead to capacity fade [23,24]. Such type of iron dissolution could be detrimental to the application of $LiFePO_4$ in HEV field.

NiP coating prepared by conventional electroless plating possess an extremely high corrosion resistance in aggressive solutions (such as in HF), and has been widely used as a protective layer to prevent the corrosion of various metals [25–27]. The previous work on NiP contained $LiFePO_4$ mainly focuses on the improvement of

* Corresponding author. Tel.: +31 15 2782480; fax: +31 15 2786730.
** Corresponding author. Tel.: +86 21 6494 2815; fax: +86 21 6494 2815.
E-mail addresses: g.song@tudelft.nl (G.-M. Song), yingwu2000@hotmail.com (Y. Wu).

0378-7753/$ – see front matter © 2010 Elsevier B.V. All rights reserved.
doi:10.1016/j.jpowsour.2009.12.089

electronic conductivity rather than on the prevention of Fe dissolution. At present, there is no report about NiP coating on $LiFePO_4$ particle surface, and its influence on preventing the dissolution of Fe is unknown.

Both of the low conductivity and Fe dissolution might be simultaneously overcome by coating the $LiFePO_4$ particles with electrical conductive and corrosion resistant NiP layer. In this paper, we will study the influence of conductive and anti-corrosion NiP nano-coating on the electrochemical properties of $LiFePO_4$ cathode as well as the dissolution of Fe in conventional $LiPF_6$ based electrolyte.

2. Experimental

Virginal $LiFePO_4$ powders were prepared by a solid-state reaction of stoichiometric amounts of CH_3COOLi (purity ≥99%), $FeC_2O_4{\cdot}2H_2O$ (purity ≥99%) and $NH_4H_2PO_4$ (purity ≥99%) obtained from Beijing Reagent Co. These reactants were thoroughly ball-mixed in a polyethylene bottle with polyethylene balls and ethanol as the grinding media for 10 h. The resulted slurry was slowly dried at 60 °C for 5 h in an oven, and then pressed into pellets. These pellets were calcined at 700 °C for 8 h in an argon atmosphere for the synthesis of $LiFePO_4$ powders. The crystal structure of the synthesized powders was analyzed by X-ray powder diffraction (XRD, Rigaku D/max 2400 with Cu Kα radiation). The $LiFePO_4$ powders were coated with NiP alloy by electroless plating. Analytical grade chemicals KIO_3 (Shanghai Chemicals, >99%), $Na_2C_6H_5O_7{\cdot}2H_2O$ (Shanghai Chemicals, >99%), $NaH_2PO_4{\cdot}6H_2O$ (Shanghai Chemicals, >99%), NH_4Cl (Beijing Reagent, >99%), $NiCl_2{\cdot}6H_2O$ (Beijing Reagent, >99%) and $NiSO_4{\cdot}6H_2O$ (Changsha Reagent, >99%) were used to prepare an electroless plating bath. The $LiFePO_4$ powders were immersed under stirring in the plating bath which contained 0.22 M $NiCl_2{\cdot}6H_2O$, 0.10 M $NiSO_4{\cdot}6H_2O$, 0.07 M $NaH_2PO_4{\cdot}6H_2O$, 0.07 M $Na_2C_6H_5O_7{\cdot}2H_2O$ and 0.8 M NH_4Cl with 5 ppm KIO_3 as the stabilizer. The plating temperature and pH value of the plating solution were 25 °C and 8–9, respectively. After plating for 8 min, the suspension was then filtered and washed using distilled water and ethanol for several times, and finally dried at 40 °C in vacuum oven. The amount of the NiP coating was measured as about 2.5 wt% of the $LiFePO_4$ powders by an inductively coupled plasma atomic emission spectrometer (ICP-AES, Leeman Profile).

The morphology and chemical composition of the $LiFePO_4$ powders were studied with a scanning electron microscope (SEM, JSM 7500F JEOL) equipped with an energy dispersive spectroscope (EDS, Roran). The nanoscale microstructure of the particles was examined using a transmission electron microscope (TEM, Philips CM30UT-FEG).

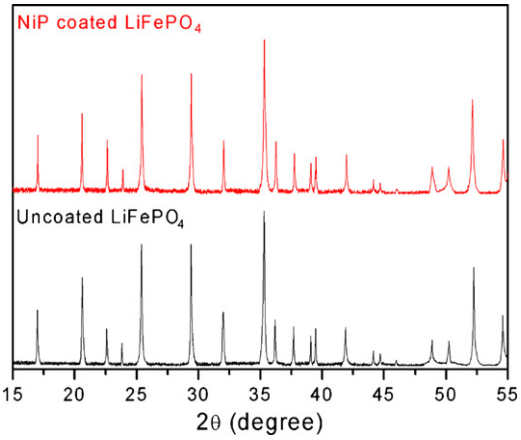

Fig. 1. The XRD patterns of NiP coated and uncoated $LiFePO_4$ powders.

The electrochemical tests were performed with 2032 coin-type cells. The cathode was prepared by pressing a mixture of 20 mg NiP coated or uncoated $LiFePO_4$ powders, 2.5 mg acetylene carbon black (Shanghai Shanshan) and 2.5 mg porous polyvinylidene fluoride (PVDF, Kynar 461) onto an Al-foil with 14 mm in diameter and 0.02 mm in thickness. The electrolyte was 1 M $LiPF_6$ dissolved in a mixture of ethylene carbonate (EC) and dimethyl carbonate (DEC) (EC:DEC = 1:1 in volume, Merck-LP40). The graphite anode with a size of 14 mm in diameter consisted of 18 mg mesocarbon microbead (MCMB 10-28 with a size of 25 μm, Osaka Gas) and 2 mg PVDF. A microporous polypropylene film (Celgard 2400) was wetted with the electrolyte and sandwiched between the cathode and anode. All cells were assembled in an argon-filled glove box. The electrochemical properties of $LiFePO_4$ were tested on a potentiostat/galvanostat system (BT-2000 Arbin Instrument Testing System) between 2.4 and 4.0 V cut-off voltage using the coin-cells. To estimate the internal resistance of the coin-cells, the electrochemical impedance spectrum (EIS) was studied with a Solatron 1287 Electrochemical Interface connected with a 1255B frequency response analyser in a range of 10 mHz to 100 kHz with an amplitude of 10 mV. The dissolution of Fe from $LiFePO_4$ cathode into $LiPF_6$ electrolyte was studied by immersing the cathodes (uncoated and coated $LiFePO_4$ powders, 50 mg) in the 1 M $LiPF_6$ in EC:DEC (1:1) electrolyte (10 mL) at 55 °C for 45 days. The dissolved

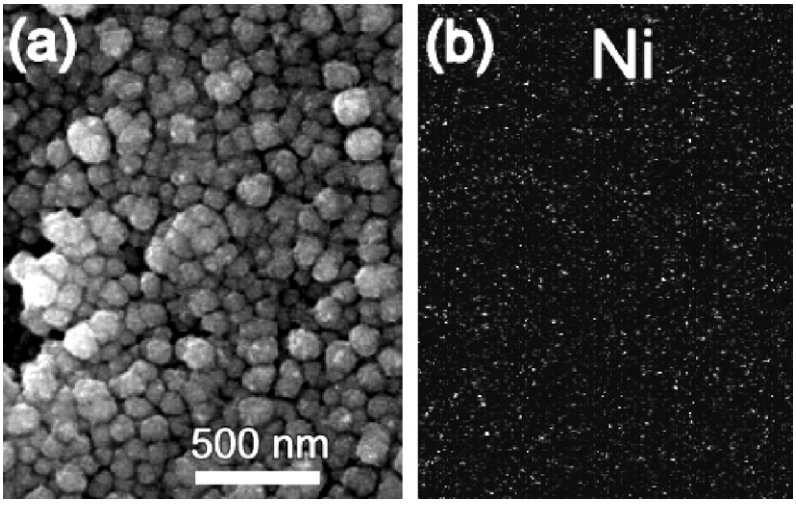

Fig. 2. SEM image of (a) NiP coated $LiFePO_4$ powders and (b) Ni element mapping.

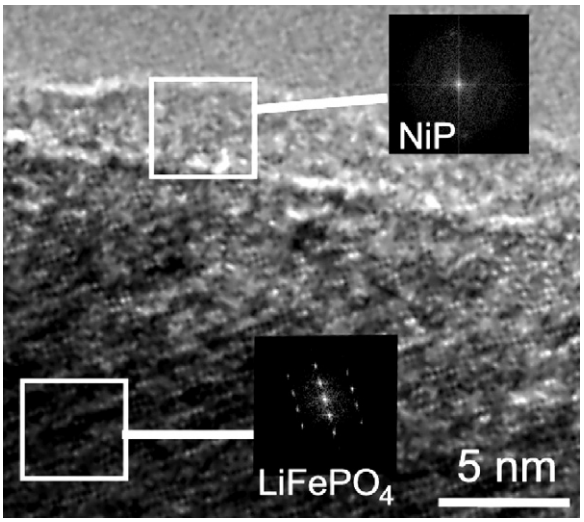

Fig. 3. High resolution TEM image of NiP coated $LiFePO_4$ particle. The Fourier transforms of the selected areas show an amorphous NiP layer on the surface of $LiFePO_4$ particle.

iron ion concentration in the electrolyte was measured with an atomic absorption spectrophotometer (AAS, Hitachi Z-5000).

3. Results and discussion

The crystalline structure of the $LiFePO_4$ does not change before and after NiP coating process, as shown by the XRD patterns (Fig. 1). The well-defined and highly intense peaks demonstrate the presence of olivine $LiFePO_4$ phase. No additional crystalline phase, like NiP compound, Li_3PO_4 [28] and Fe_2P [20] impurities, is detected in these XRD patterns. It means that the synthesized $LiFePO_4$ powders have high purity. Fig. 2(a) shows the morphology of the NiP coated $LiFePO_4$ powders. The average particle size of the spherical particles is about 100 nm. Elemental mapping analysis shows the presence of Ni (Fig. 2(b)). The high resolution transmission electron microscope (HRTEM) image (Fig. 3) of the NiP coated $LiFePO_4$ powders shows an disordered layer with a thickness of about 5 nm covering on a crystalline particle. The Fourier transforms of the selected areas in disordered layer and crystalline particle in the HRTEM image show that the disordered layer is amorphous and the particle is $LiFePO_4$. The amorphous layer becomes thick when the NiP content increases. The present electroless plating method has been widely used to prepare NiP coatings in the past twenty years [24–27,29,30]. So, the deposited disorder layer on $LiFePO_4$ particles should be amorphous NiP layer. This result also can explain the absence of the NiP coating in the XRD pattern of the coated $LiFePO_4$ due to the amorphous feature of the coating.

For the charge/discharge test, all the cells were charged at a constant current rate of 0.1 C (1 C = 170 mA g^{-1}) at 25 °C, and discharged at different current rates from 0.1 to 5 C. Fig. 4 shows first few charge/discharge profiles of the uncoated and NiP coated $LiFePO_4$ cells at a low charge/discharge rate of 0.1 C. Both of the $LiFePO_4$ show typical flat curves for charge reaction and discharge reaction over a large compositional range (redox reaction between $LiFePO_4$ and $FePO_4$). Small polarization and high reversible capacity around 150–153 mAh g^{-1} for both of the $LiFePO_4$ are observed, which is probably caused by the fine particle size (about 100 nm; see Fig. 2). Any way, the NiP coated $LiFePO_4$ still shows a slight higher charge and discharge capacity than the uncoated $LiFePO_4$ although the rate is as low as 0.1 C. When the discharge current rate increases, the difference between the NiP coated and uncoated $LiFePO_4$ becomes remarkable, as shown in Fig. 5. The discharge capacities of the uncoated $LiFePO_4$ decreases much faster than that of the coated

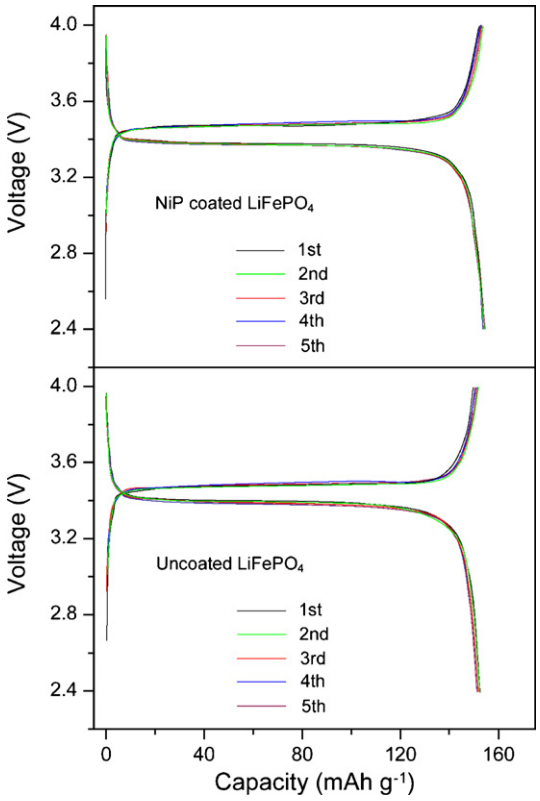

Fig. 4. First five charge/discharge voltage profiles of the NiP coated and uncoated $LiFePO_4$ cells at a 0.1 C charge/discharge rate at 25 °C.

$LiFePO_4$. At a current density of 5 C, a higher capacity of 120 mAh g^{-1} is tested on the NiP coated $LiFePO_4$. The voltage plateau of the NiP coated $LiFePO_4$ is significantly lengthened compared with that of the uncoated $LiFePO_4$ at the high discharge current rates, which should be attributed to the lower polarization of the $LiFePO_4$ during the electrochemical reaction after coating. The above evidence demonstrates that the rate performance of NiP coated $LiFePO_4$ is much superior to that of uncoated $LiFePO_4$. Electronic conductive NiP coating forms a conductive network connecting all $LiFePO_4$ particles and completely filling some of the voids, consequently improves the electronic conductivity of $LiFePO_4$. Such a conductive network also exists on the previous carbon coated $LiFePO_4$, and

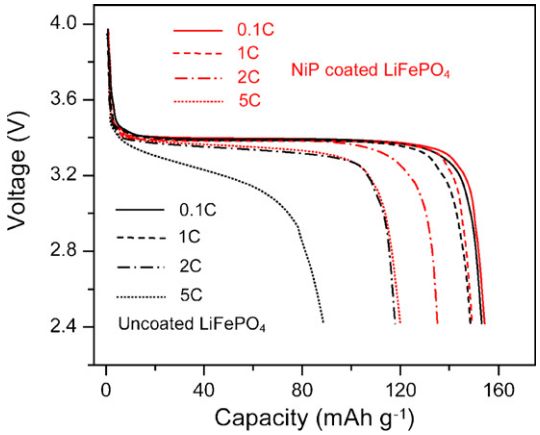

Fig. 5. Discharge profiles of uncoated and NiP coated $LiFePO_4$ cells under 0.1 C charge rate and 0.1–5 C discharge rate at 25 °C. The red lines represent the NiP coated $LiFePO_4$, and the black lines represent uncoated $LiFePO_4$. (For interpretation of the references to color in this figure legend, the reader is referred to the web version of the article.)

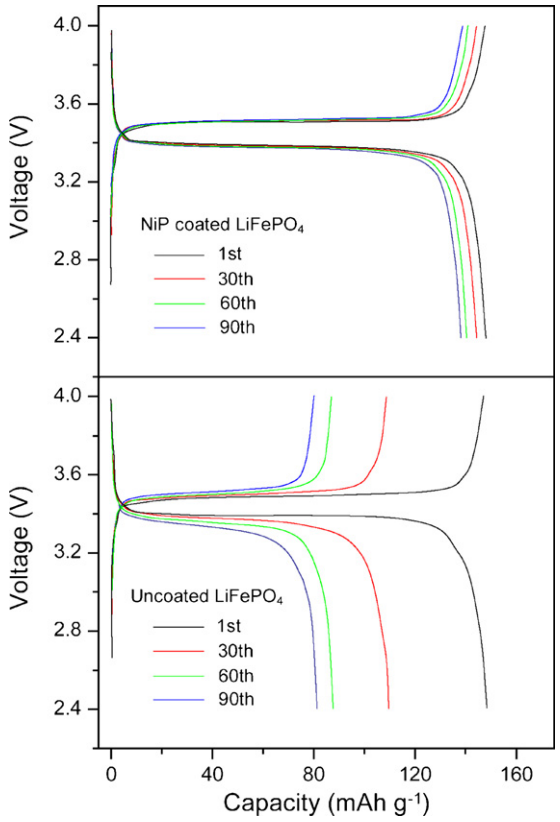

Fig. 6. Cycling performance of uncoated and NiP coated $LiFePO_4$ cells under 0.1 C charge rate and 1 C discharge rate at 55 °C.

metallic phases like Fe or Ni phosphide and NiP contained $LiFePO_4$ [14,18–20,31,32]. Such a conductive web enhances the diffusion of lithium ion in a solid phase and electron jumping across a poorly conducting compound, and consequently the diffusion kinetics is improved and a good rate performance is achieved.

Fig. 6 illustrates the cycle characteristics of the uncoated and NiP coated $LiFePO_4$ at 55 °C under 0.1 C charge rate and 1 C discharge rate. The maximum discharge capacity for the uncoated $LiFePO_4$ is 149 mAh g^{-1}, and dramatically decreases to 81 mAh g^{-1} after 100th cycles. On the contrary, the maximum capacity of the NiP coated $LiFePO_4$ is 151 mAh g^{-1}, and is well maintained at 140 mAh g^{-1} after 100 cycles, exhibiting a good capacity retention of 93% after 100 cycles. Fig. 7 presents the charge/discharge profile evolution

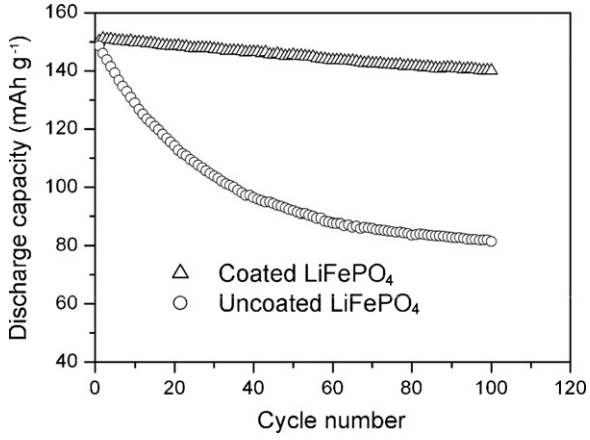

Fig. 7. Charge/discharge voltage profiles of the NiP coated and uncoated $LiFePO_4$ under 0.1 C charge rate and 0.1–5 C discharge rate at 55 °C.

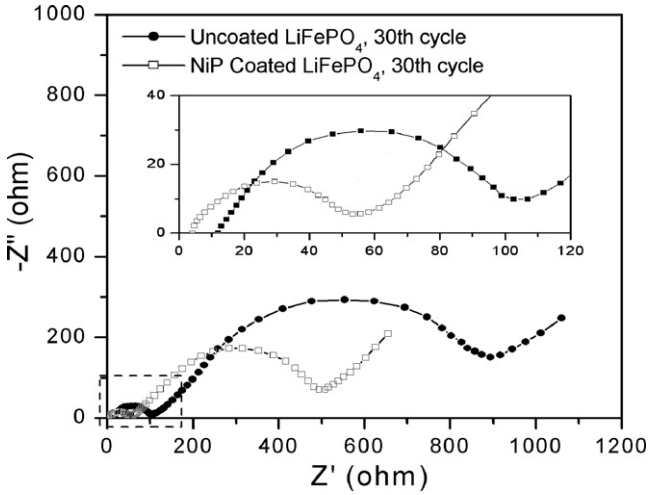

Fig. 8. EIS spectra of uncoated and NiP coated $LiFePO_4$ against graphite anodes at 30th cycle. The insert represents expands views for the high-to-medium frequency region.

of several cycles of the NiP coated and uncoated $LiFePO_4$. It is clear that the charge/discharge capacity fade of the uncoated $LiFePO_4$ becomes more pronounced with cycling compared the NiP coated $LiFePO_4$. This evidence indicates that the NiP coated $LiFePO_4$ has a better elevated temperature cycleability than the uncoated $LiFePO_4$ against graphite anode.

To understand the capacity fade of $LiFePO_4$, the EIS was performed. We choose graphite anode rather than lithium anode because the dissolution of iron is easily detected with graphite anode [33]. The Nyquist plots of both uncoated $LiFePO_4$ and NiP coated $LiFePO_4$ charged to 4.0 V at the 30th cycle are shown in Fig. 8. Each plot has two depressed semicircles: one semicircle is in the high-to-medium frequency region and is attributed to the resistance of surface film (R_f) covering on the $LiFePO_4$ cathode and graphite anode, and the other in the low frequency region approximately represents the charge transfer resistance (R_{ct}). The intercept at the Z' axis in high frequency represents the bulk resistance of the electrolyte (R_b). The incline line in the low frequency is associated with the Li-ion diffusion in the $LiFePO_4$ particles and represents the Warburg impedance (W) [34,35]. The values of R_f and R_{ct} of the uncoated $LiFePO_4$ cell are 91, 790 Ω at, respectively, both of them are higher than that of the NiP coated $LiFePO_4$ cell (51 and 439 Ω). This result shows that the charge transfer resistance plays the predominant role in governing the Li-ion transport in both NiP coated and uncoated $LiFePO_4$ cells, and the NiP coating significantly suppress the rise of both of the surface film resistance and charge transfer resistance upon elevated temperature cycling. There are two possible reasons for the increase in impedance: (1) chemical reaction at the electrode surface which might results in the formation and thickening of SEI upon cycling; (2) the crystalline structure of $LiFePO_4$ cathode material might be destroyed during cycling. The previous investigation of Amine et al. [21] on the capacity fade of $LiFePO_4$ against graphite anode shows that interfacial impedance of the graphite anode remarkably increased due to the dissolution of Fe from $LiFePO_4$ and the subsequent deposition on the graphite anode surface, which catalysed the formation of interfacial films on the graphite anode. The passivation layer on graphite anode is ionic conductor and electronic insulator [36], the reduction of dissolved Fe as metallic Fe in the SEI of the anode increases the electronic conductivity of the passivation layer as well as catalyses the formation of the SEI [24,33]. As a result, the SEI growth is accelerated, the interfacial impedance between the electrolyte and graphite anode increases, and therefore the diffusion kinetics deteriorates. It is well

known that the NiP coating has a good corrosion resistance in acidic solution, like HF [37]. The previous work of Sun et al. [38] shows that AlF_3 coating on $LiCoO_2$ can remarkable suppress the dissolution of Co in $LiPF_6$ electrolyte solution by preventing the attack of the trace HF in the electrolyte on the active particles. Herein, we expect that the NiP coating could work as a protective layer on the $LiFePO_4$ particles to prevent the direct contact of the trace HF in $LiFP_6$ based electrolyte from the active $LiFePO_4$ so as to decrease the dissolution of Fe. The concentration of Fe^{2+} ion dissolved in the 1 M $LiPF_6$ in EC:DEC (1:1 volume) electrolyte after storing the $LiFePO_4$ in the electrolyte at 55 °C for 45 days is 11 ppm for the NiP coated $LiFePO_4$, which is only about 1% of the Fe^{2+} ion concentration (1265 ppm) for the uncoated $LiFePO_4$. This result confirms that the NiP coating can greatly decrease the dissolution of Fe of $LiFePO_4$ in $LiPF_6$ based electrolyte. Therefore, the interfacial impedance between the graphite anode and the electrolyte (mainly caused by the formation and growth of the SEI layer [21]) will be greatly reduced. The present result is consistent with the previous result of Amine et al. [21,38]. It is reasonably believed that NiP layer on the cathode particle can effectively suppress the formation of LiF (probably produced by the reaction of cathode with trace HF [39]) in the surface film at the $LiFePO_4$ cathode surface by working as a protective layer for preventing the reaction between the active cathode and the electrolyte so as to inhibit the formation of the surface layer on the cathode. The surface layer on the cathode probably contains variable salt-based LiF, Li_xPOF_y, etc. [40], in which LiF is highly resistive to Li^+ ion transport [41]. Thus the suppression of the formation of LiF can directly inhibit the increase of cathode/electrolyte interfacial impedance. Additionally, the electronic NiP network increases the electronic conductivity of $LiFePO_4$. Both lead the decrease of the cathode/electrolyte interfacial impedance. So, both of the interfacial impedances of the graphite anode and $LiFePO_4$ cathode are reduced due to the presence of NiP. Therefore, the impedance of the NiP coated $LiFePO_4$ is lower than that of uncoated $LiFePO_4$ cell after long-term cycling, as shown in Fig. 8.

Besides improving the conductivity of $LiFePO_4$ and preventing the dissolution of Fe from $LiFePO_4$, the NiP coating could also sustain the structure stability of $LiFePO_4$ upon cycling because NiP coating has a good metallic mechanical property [37,42], similar to ZrO_2 coating [43]. NiP coating should mitigate the volume change during the insertion/desertion of Li ion in $LiFePO_4$ which can be up to 6.64% when a fully charged state is approached [43]. Consequently, the mechanical fatigue of $LiFePO_4$ is suppressed by the NiP coating.

4. Conclusions

An amorphous conductive metallic NiP nano-coating was successfully deposited on the surfaces $LiFePO_4$ particles via a simple electroless plating at room temperature. The NiP coating plays a key role in decreasing the interfacial impedance and preventing the dissolution of Fe upon elevated temperature cycling by working as a conductive and protective layer of the active $LiFePO_4$. Both the rate performance and elevated temperature cycleability of $LiFePO_4$ against graphite anode are simultaneously improved. This evidence shows that the surface modification with metallic NiP nano-coating is a promising approach to improve the rate performance and elevated temperature cycleability of $LiFePO_4$.

Acknowledgements

This work was partially financial supported by the Program of Professor of Special Appointment (Eastern Scholar) at Shanghai Institutions of Higher Learning and Innovation Program of Shanghai Municipal Education Commission, P.R. China.

References

[1] L. Laffont, C. Delacourt, P. Gibot, M.Y. Wu, P. Kooyman, C. Masquelier, J.M. Tarascon, Chem. Mater. 18 (2006) 5520.
[2] C. Delacourt, P. Poizot, J.M. Tarascon, C. Masquelier, Nat. Mater. 4 (2005) 254.
[3] G.M. Song, Y.J. Wang, Y.K. Guo, Y. Zhou, W.Y. Zhou, Rare Met. Mater. Eng. 30 (2001) 299.
[4] S.S. Zhang, K. Xu, T.R. Jow, J. Power Sources 159 (2006) 702.
[5] G.M. Song, Y.J. Wang, Y. Zhou, J. Power Sources 128 (2004) 270.
[6] G.M. Song, Z.M. Xu, Y.J. Wang, Y. Zhou, Electrochem. Commun. 5 (2003) 907.
[7] J. Hassoun, P. Reale, B. Scrosati, J. Mater. Chem. 17 (2007) 3668.
[8] S.Y. Chung, J.T. Bloking, Y.M. Chiang, Nat. Mater. 1 (2002) 123.
[9] A.S. Andersson, J.O. Thomas, J. Power Sources 97–98 (2001) 498.
[10] C.M. Burba, R. Frech, J. Power Sources 172 (2007) 870.
[11] S. Franger, F. Le Cras, C. Bourbon, H. Rouault, Electrochem. Solid-State Lett. 5 (2002) A231.
[12] H. Liu, J.Y. Xie, K. Wang, J. Alloy Compd. 459 (2008) 521.
[13] N. Ravet, Y. Chouinard, J.F. Magnan, S. Besner, M. Gauthier, M. Armand, J. Power Sources 97–98 (2001) 503.
[14] C.H. Mi, X.B. Zhao, G.S. Cao, J.P. Tu, J. Electrochem. Soc. 152 (2005) A483.
[15] H. Huang, S.C. Yin, L.F. Nazar, Electrochem. Solid-State Lett. 4 (2001) A170.
[16] Z.G. Lu, H. Cheng, M.F. Lo, C.Y. Chung, Adv. Funct. Mater. 17 (2007) 3885.
[17] F. Croce, A.D. Epifanio, J. Hassoun, A. Deptula, T. Olczac, B. Scrosati, Electrochem. Solid-State Lett. 5 (2002) A47.
[18] C.S. Li, S.Y. Zhang, F.Y. Cheng, W.Q. Ji, J. Chen, Nano Res. 1 (2008) 242.
[19] P.S. Herle, B. Ellis, N. Coombas, L.F. Nazar, Nat. Mater. 3 (2004) 147.
[20] C.W. Kim, J.S. Park, K.S. Lee, J. Power Sources 163 (2006) 144.
[21] K. Amine, J. Liu, I. Belharouak, Electrochem. Commun. 7 (2005) 669.
[22] M. Koltypin, D. Aurbach, L. Nazar, B. Ellis, Electrochem. Solid-State Lett. 10 A (2007) 40.
[23] H.C. Wu, C.Y. Su, D.T. Shieh, M.H. Yang, N.L. Wu, Electrochem. Solid-State Lett. 9 A (2006) 537.
[24] K. Zaghib, N. Ravet, M. Gauthier, F. Gendron, A. Mauger, J.B. Goodenough, C.M. Julien, J. Power Sources 163 (2006) 560.
[25] B.P. Zhang, E. Akiyama, H. Habazaki, A. Kawashima, K. Asami, K. Hashimoto, Mater. Sci. Eng. A181/A182 (1994) 1114.
[26] R.J.C. Brown, P.J. Brewer, M.J.T. Milton, J. Mater. Chem. 12 (2002) 2749.
[27] Y.J. Chen, M.S. Cao, Q. Xu, J. Zhu, Surf. Coat. Technol. 172 (2003) 90.
[28] S.J. Kwon, C.W. Kim, W.T. Jeong, K.S. Lee, J. Power Sources 137 (2004) 93.
[29] Y.Z. Zhang, Y.Y. Wu, K.N. Sun, M. Yao, J. Mater. Sci. Lett. 17 (1998) 119.
[30] T. Osaka, M. Usuda, I. Koiwa, H. Sawai, Jpn. J. Appl. Phys. 10 (1988) 1885.
[31] C. Delacourt, P. Poizot, J.M. Tarascon, C. Masquelier, Electrochem. Solid-State Lett. 9 (2006) A352.
[32] A. Guerfi, S. Duchesne, Y. Kobayashi, A. Vijh, K. Zaghib, J. Power Sources 175 (2008) 866.
[33] H.H. Chang, C.C. Chang, C.Y. Su, H.C. Wu, M.H. Yang, N.L. Wu, J. Power Sources 185 (2008) 466.
[34] Y.J. Liu, X.H. Li, H.J. Guo, Z.X. Wang, W.J. Peng, J. Power Sources 184 (2008) 522.
[35] E. Barsoukov, J.H. Kim, J.H. Kim, C.O. Yoon, H. Lee, Solid State Ionics 116 (1999) 249.
[36] R.S. Rubino, E.S. Takeuchi, J. Power Sources 81–82 (1999) 373.
[37] W. Sha, J.S. Pan, J. Alloys Compd. 128 (1992) L1.
[38] Y.K. Sun, J.M. Han, S.T. Myung, W.S. Lee, K. Amine, Electrochem. Commun. 8 (2006) 821.
[39] D. Aurbach, B. Markovsky, G. Salitra, E. Markevich, Y. Talyossef, M. Koltypin, L. Nazar, B. Ellis, D. Kovacheva, J. Power Sources 165 (2007) 491.
[40] A.M. Anderson, D.P. Abraham, R. Haasch, S. MacLaren, J. Liu, K. Amine, J. Electrochem. Soc. 149 (2002) A1358.
[41] S. Seki, Y. Kobayashi, H. Miyashiro, A. Yamanaka, Y. Mita, T. Iwahori, J. Power Sources 146 (2005) 741.
[42] A. Grosjeana, M. Rezrazi, J. Takadoumb, P. Bercot, Surf. Coat. Technol. 137 (2001) 92.
[43] H. Liu, G.X. Wang, D. Wexler, J.Z. Wang, H.K. Liu, Electrochem. Commun. 10 (2008) 165.